RANDOM FOREST CLASSIFICATION FOR MANGROVE CANOPY COVER SPATIAL ANALYSIS IN BENOA BAY – BALI, INDONESIA

Nanin Anggraini[a,b]*, Noverita Dian Takarina[c], Ratih Dewanti Dimyati[d], Dwi Nowo Martono[a], Evi Frimawaty[a], Rahmadi[d], A. A. Md. Ananda Putra Suardana[b]

[a] Department of Environmental Science, Graduate School of Sustainable Development, University of Indonesia, Jakarta, 10430, Indonesia
[b]Research Center for Ecology, National Research and Innovation Agency (BRIN), Cibinong, 16911, Indonesia
[c]Department of Biology, Faculty of Mathematics and Natural Sciences, Universitas Indonesia, Depok 16424, Indonesia
[d]Research Center for Geoinformatics, National Research and Innovation Agency (BRIN), Bandung, 40135, Indonesia

email: *nani011@brin.go.id

Received: 15-09-2025; Revised: 10-10-2025; Approved: 19-12-2025

Abstract. Mangrove forests play an essential role in maintaining the stability of coastal ecosystems by providing habitat for various species, protecting shorelines, and as a carbon source. The presence of mangrove areas can be monitored using land-cover information derived from remote sensing data using the Random Forest (RF) classification method, enabling practical ecosystem assessment and management. This study aims to develop and evaluate an RF classification model to produce accurate spatial information about mangrove canopy cover. The study area, Benoa Bay in Bali, Indonesia, is known for its dynamic and ecologically complex mangrove habitat. Inputs for the RF classification are bands on Sentinel-2A satellite imagery, Mangrove Vegetation Index (MVI), Normalized Difference Vegetation Index (NDVI), Enhanced Mangrove Index (EMI), Modified Normalized Difference Water Index (MNDWI), Normalized Difference Moisture Index (NDMI), and Normalized Difference Salinity Index (NDSaII), along with topographic variables such as elevation and slope with two treatments namely RF with DEM + Slope (DS) and RF without DEM + Slope (wDS). Model validation was conducted using high-resolution imagery from Google Earth Pro and the 2024 National Mangrove Map. Coastal land cover classification was divided into water, mangrove, open land, built-up land, and non-mangrove vegetation. In general, the results of RF classification with different treatments (DS, wDS) had very high accuracy, as evidenced by Overall Accuracy exceeding 90% and a Kappa value exceeding 90%, indicating the model's consistency and reliability in capturing spatial variations in land cover. Similarly, the accuracy of mangrove canopy cover classification based on the national mangrove map was more than 90% and the kappa value was more than 80%. These findings demonstrate the robustness of the RF model and its potential to support data-driven coastal management practices.

Keywords: *Random Forest; mangrove; Benoa Bay*.

1 INTRODUCTION

Random Forest (RF) is a widely used ensemble classifier that builds multiple decision trees to enhance prediction stability and reliability, particularly in spatial and remote sensing contexts. Unlike parametric methods, RF does not require assumptions about the underlying data distribution, which makes it highly adaptable for processing complex datasets such as satellite imagery with diverse spectral and spatial characteristics (Belgiu & Drăguț, 2016; Biau & Scornet, 2016; Immitzer et al., 2012). This algorithm consistently achieves higher classification accuracy in land cover studies, especially when augmented with multi-temporal and textural variables, yielding accuracy

improvements ranging from 10% to 30% in specific land cover types (Breiman, 2001; Elmahdy et al., 2020; Nandika et al., 2023; Rodriguez-Galiano et al., 2012).

RF is well-regarded for its ability to manage multicollinearity and effectively process large, high-dimensional datasets. In addition, it offers internal measures of predictor significance, which are frequently applied in feature selection processes within spatial modeling tasks (Belgiu & Drăguț, 2016). Given these capabilities, RF holds strong promise for enhancing the accuracy of spatial mapping applications, including mangrove canopy cover classification.

RF has become a widely adopted approach for mapping mangrove distribution using multispectral satellite imagery, largely due to its classification accuracy and computational efficiency. One of RF's advantages is its compatibility with cloud-based platforms such as Google Earth Engine (GEE), which facilitates rapid and scalable remote sensing analysis over large areas. For example, a research in Hara, Iran, utilizing combined Sentinel-1 and Sentinel-2 data, reported that RF achieved an overall accuracy of 93.23% and a Kappa coefficient of 0.92 when distinguishing mangrove, tidal flats, and open water (Giri, 2023). Similarly, research conducted in Pakistan used RF within the GEE environment to assess mangrove cover changes from 1990 to 2020, achieving over 90% accuracy with Landsat 30 m imagery (Gilani et al., 2021). Moreover, RF has consistently outperformed alternative classifiers, such as kernel logistic regression and Naïve Bayes, in global-scale mangrove mapping efforts, with reported F1 scores exceeding 0.90 in multiple studies using both medium- and high-resolution data (Elmahdy et al., 2020).

Accurate mapping of mangrove canopy cover is essential for understanding the spatial distribution and structural complexity of coastal vegetation. Mangrove ecosystems serve crucial ecological, economic, and social functions, particularly due to their role as highly efficient carbon sinks. Studies have shown that mangroves can store carbon at levels three to five times greater than most terrestrial forest types (Donato et al., 2011; Kauffman et al., 2020; Murdiyarso et al., 2015; Tomlinson, 2016). A significant portion of this carbon—up to 77.9%—is found within mangrove biomass components such as tree trunks, foliage, and sediment layers (Bachmid et al., 2018).

Globally, the estimated average carbon stock in mangrove ecosystems is approximately 1,023 Mg C/ha (Donato et al., 2011), while Indonesia's mangroves store an average of about 891.70 tons per hectare. The total potential carbon stock across Indonesian mangroves is estimated at 2.89 Tt C (Wahyudi et al., 2018). In the context of carbon financing, this surplus represents a valuable opportunity: Indonesian mangroves could contribute up to 3.14 PgC, equivalent to approximately Rp 220 trillion, assuming a carbon market price of US$5 per ton. (Murdiyarso et al., 2015). From an economic perspective, the annual ecosystem service value of mangrove forests is estimated to exceed US$50,000 per hectare for local coastal communities (Mukherjee et al., 2014).

The ability of mangroves to sequester and store carbon significantly contributes to the fulfillment of Sustainable Development Goal (SDG) 13, which focuses on Climate Action. Beyond their climate mitigation potential, mangroves offer a wide array of ecosystem services that align with multiple other SDGs. These include their contributions to poverty reduction (SDG 1), food security (SDG 2), access to clean water (SDG 6), promotion of sustainable livelihoods (SDG 8), resilience in coastal urban areas (SDG 11), marine ecosystem health (SDG 14), and the protection of terrestrial ecosystems (SDG 15) (Anggraeni, 2024; Friess et al., 2019; Gong et al., 2024; Sasmito et al., 2023).

Benoa Bay, located in Bali, Indonesia, has a mangrove forest of approximately 1,373.50 hectares (As-syakur et al., 2025; Yastika et al., 2019). This area lies in close proximity to dense human activities, including residential neighborhoods, industrial facilities, airport infrastructure, commercial zones, and reclaimed coastal lands, placing it under constant environmental pressure (Sugianthi et al., 2007). As such, consistent monitoring is essential to support long-term mangrove ecosystem sustainability.

The use of Sentinel-2A satellite imagery has proven effective for detecting mangrove cover due to its high temporal and spatial resolution. The satellite captures imagery

at resolutions of 10, 20, and 60 meters across various multispectral bands, along with a 10-meter panchromatic band and a revisit frequency of every five days. Sentinel-2A includes 13 spectral bands that cover the visible, NIR, and SWIR regions of the electromagnetic spectrum (ESA, 2025). This wide spectral range, when combined with suitable classification techniques, enables the extraction of detailed and reliable land cover information.

This research aims to develop and evaluate a RF classification model to produce accurate spatial information on mangrove canopy cover, thereby supporting sustainable coastal management. The research gap in this study is the challenge of mangrove canopy classification, which is often hindered by spectral overlap with other coastal vegetation. Therefore, an adaptive and robust machine learning approach, such as RF, that combines multi-source data with relevant spectral and textural features is required. RF has weaknesses in classifying high-resolution data with complex spectral and spatial features, as it can be challenging to separate similar features in such datasets (Breiman, 2001). Furthermore, multi-temporal mangrove cover detection requires careful attention, as mangrove sites differ from terrestrial vegetation and are strongly influenced by tides. Determining balanced training samples for each land cover class is necessary to reduce class imbalance and spatial leakage caused by the inclusion of training areas during testing. Therefore, attention and precision are required when determining the location of the training area to produce accurate information.

2 MATERIALS AND METHODOLOGY

2.1 Location and Data

This research was carried out in the mangrove ecosystem of Benoa Bay, located in southern Bali, Indonesia, within the geographic coordinates of 08°41'–08°47' S and 115°10'–115°15' E (Figure 2-1). The area extends across both Badung Regency and Denpasar City, covering several coastal villages, namely Sesetan, Pemogan, Serangan, and Sidakarya (As-syakur et al., 2025; Danaparamita, 2020; Loviasari et al., 2017). Geomorphologically, Benoa Bay is a semi-enclosed estuarine environment, shaped by the interaction of river systems—particularly the Badung and Mati rivers—and heavily influenced by surrounding human activities, including port operations and tourism development (As-syakur et al., 2025). The region falls within a tropical monsoon climate zone, receiving an average annual rainfall of approximately 1,803 mm. Air temperatures typically range between 24.0 °C and 27.5 °C throughout the year, with an annual mean of about 27.6 °C. Relative humidity levels tend to fluctuate between 80% and 85%, while the peak of the rainy season occurs during December and January, during which monthly precipitation may reach 250–296 mm (As-syakur et al., 2025; *Bali (Denpasar) Climate (Indonesia): Data and Graphs for Weather & Climate In Bali (Denpasar)*, 2025).

The data used in this study are a mosaic of Sentinel 2A Surface Reflectance images for the period January - December 2024, provided by the European Space Agency (ESA), with atmospheric correction already applied. Sentinel-2 offers 13 spectral bands, captured at spatial resolutions of 10, 20, and 60 meters, and revisits the same location every 5 to 7 days (Table 2-1) (ESA, 2025). This combination of high spectral and temporal resolution makes it particularly suitable for vegetation monitoring in dynamic coastal ecosystems. In addition to utilizing satellite-derived imagery, this research used the 2024 National Mangrove Map—issued by (Ministry of Forestry, 2025)—as an external reference to validate the accuracy of mangrove canopy cover derived from the RF classification.

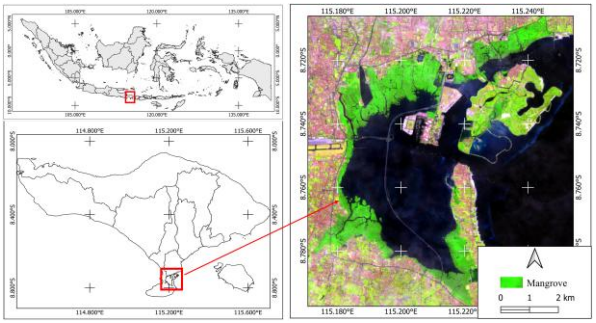

Figure 2-1: Benoa Bay Bali, Indonesia

Table 2-1: Sentinel-2A Data Specifications (Esa, 2025)

Resolusi Spektral (nm)	Resolusi Spasial
B2: Blue (~493 nm) B3: Green (~560 nm)	10

B4: Red (~665 nm) B8: NIR (~833)	
B5: Vegetation Red Edge (~704nm) B6: Vegetation Red Edge (~740nm) B7: Vegetation Red Edge (~783nm) B8A: Vegetation Red Edge (~865nm) B11: SWIR (~1610nm) B12: SWIR dan (~2190nm)	20
B1: Coastal Aerosol (~443nm) B9: Water Vapour (~945 nm) B10: Cirrus band (~1374 nm)	60

This study also used a 30 m resolution SRTM (Shuttle Radar Topography Mission) Digital Elevation Model (DEM) from NASA, which provides elevation and slope information used as boundary data to determine mangrove growth locations. Alongi (2002) and Komiyama et al. (2008) state that mangroves grow on land at elevations of 0-5 m above sea level. In addition, data from the 2024 National Mangrove Map of the Ministry of Forestry were used as accuracy test data for the mangrove information derived from the classification process.

2.2 Methods

The methodological workflow in this research consists of four main stages: data acquisition and preprocessing, sample area definition, RF classification, and accuracy evaluation. All data-related processes were conducted using the cloud-based GEE platform.

1) Data Acquisition and Preprocessing: Sentinel-2A imagery was filtered to minimize cloud contamination by applying cloud masking based on the Quality Assessment (QA) band available in GEE, ensuring optimal imagery for analysis. Cloud separation is performed to obtain image data under minimal cloud conditions using Cloud Probability in Sentinel-2 (Sen2Cor) on the GEE platform. The Sen2Cor method uses QA60 band to identify cloud-affected pixels based on the value in the 10th bit. Pixels with a value of 1 in the 10th bit are identified as clouds and cloud shadows, while a value of 0 is identified as cloud-free pixels.

2) Sample Selection: The number of samples was determined using the Slovin method, which is calculated based on the number of pixels in the image data. The stratified spatial split method was also used to prevent spatial leakage, dividing the data into 70% for modeling and 30% for accuracy testing, as reported by Nandika et al. (2023). The research location had 1,351,322 pixels, and with an α value of 0.5, the minimum number of samples required was 400 pixels. In this study, the number of training samples was 10,406, and the number for accuracy testing was 4,354. The training area for RF classification was 105, evenly distributed across the research location (Table 2-2).

Table 2-2. Number of Training Area Polygons

Training Area	Number of Poligons
Water	30
Mangrove	32
Open land	13
Build up	11
Non Mangrove Vegetation	19

3) RF Classification: Input features for the RF classifier included selected spectral bands from Sentinel-2A (Blue, Green, Red, Red Edge bands 5, 6, 7, NIR, and SWIR bands 11 and 12), as well as several mangrove-related spectral indices: MVI, NDVI, EMI, MNDWI, NDMI, and NDSaII (Table 2-3). The features used in this RF include vegetation spectral reflectance, canopy structure, water content, relevant thermal-mineral conditions in the mangrove ecosystem in the intertidal zone, canopy humidity, salinity, water bodies, and settlements, so that it can separate mangroves from other land covers.

RF classification uses 200 trees with Variable presplit: 6, Meanleaf population: 5, Bag fraction: 0.7, Max nodes: 500. The RF classification process is carried out using two treatments, namely using DEM + Slope (DS), and without using DEM + Slope (wDS). The results of the RF classification will be classified into water bodies, mangroves, open land, built-up land, and non-mangrove vegetation, which are defined as follows (Table 2-4).

A limitation of this study is that it has not yet used tidal data as input for RF classification. Tidal data will be considered for use as input for RF classification in future studies.

Table 2-3: Index for R

Index	Algorithm on Sentinel 2A	References
$MVI = \frac{(NIR - Green)}{(SWIR1 - Green)}$	$MVI = \frac{(Sentinel_{B8} - Sentinel_{B3})}{(Sentinel_{B11} - Sentinel_{B3})}$	(Baloloy et al., 2020)
$NDVI = \frac{(NIR - Red)}{(NIR + Red)}$	$NDVI = \frac{(Sentinel_{B8} - Sentinel_{B4})}{(Sentinel_{B8} + Sentinel_{B4})}$	(Kuenzer et al., 2011)
$EMI = \frac{(NIR - SWIR_{1500-1800})}{(NIR + Green)}$	$EMI = \frac{(Sentinel_{B8} - Sentinel_{B11})}{(Sentinel_{B11} + Sentinel_{B3})}$	(Prayudha et al., 2024)
$MNDWI = \frac{(Green - SWIR)}{(Green + SWIR)}$	$MNDWI = \frac{(Sentinel_{B3} - Sentinel_{B11})}{(Sentinel_{B3} + Sentinel_{B11})}$	(Xu, 2006)
$NDMI = \frac{(NIR - SWIR)}{(NIR + SWIR)}$	$NDMI = \frac{(Sentinel_{B8} - Sentinel_{B11})}{(Sentinel_{B8} + Sentinel_{B11})}$	(Purwanto et al., 2022)
$NDSaII = \frac{(Red - NIR)}{(Red + NIR)}$	$NDSaII = \frac{(Sentinel_{B4} - Sentinel_{B8})}{(Sentinel_{B4} + Sentinel_{B8})}$	(Purwanto et al., 2022)

Table 2-4. Land Cover Class Description

Land Cover Class	Description
Water	Rivers, ponds, sea
Mangrove	Natural mangroves, rehabilitated mangroves
Open land	Open ground, sand
Build up	Residential, industrial, office areas
Non Mangrove Vegetation	Rice fields, plantations, scrubland, forests, grasslands

Source: Castillo et al. (2021) modified

4) Accuracy Assessment: To evaluate the performance of the classification model, accuracy assessment was carried out using a confusion matrix approach. This method enables the calculation of four key metrics *(Congalton, 1991)*: Producer's Accuracy (PA), User's Accuracy (UA), Overall Accuracy (OA), and the Kappa Coefficient (KA). Validation data were obtained from high-resolution imagery available via Google Earth Pro. PA reflects the proportion of reference samples correctly classified for each class and is commonly used to assess omission errors.

UA indicates the likelihood that a pixel classified into a certain category actually represents that category on the ground, addressing commission errors. OA provides the ratio of correctly classified pixels to the total number of reference pixels used. The KA offers a statistical measure that accounts for agreement occurring by chance and considers both omission and commission errors.

$$PA = \left(\frac{X_{ii}}{X_{i+}}\right) * 100\% \quad (1)$$

$$UA = \left(\frac{X_{ii}}{X_{i}}\right) * 100\% \quad (2)$$

$$OA = \frac{\sum_{i=1}^{r} X_{ii}}{N} * 100\% \quad (3)$$

$$KA = \frac{N\sum_{i=1}^{r} X_{ii} - \sum_{i=1}^{r}(X_{i+} * X_{+i})}{N^2 - \sum_{i=1}^{r}(X_{i+} * X_{+1})} * 100\% \quad (4)$$

where:

N : Total number of pixels in the area
X_{ii} : Diagonal value of the contingency matrix at row i and column i
X_{+i} : Total number of pixels in column i
X_{i+} : Total number of pixels in row i

In addition to the confusion matrix evaluation, the mangrove cover classification was further validated using the 2024 National Mangrove Map issued by Ministry of Forestry (2025). A complete overview of the research workflow is illustrated in Figure 2-2.

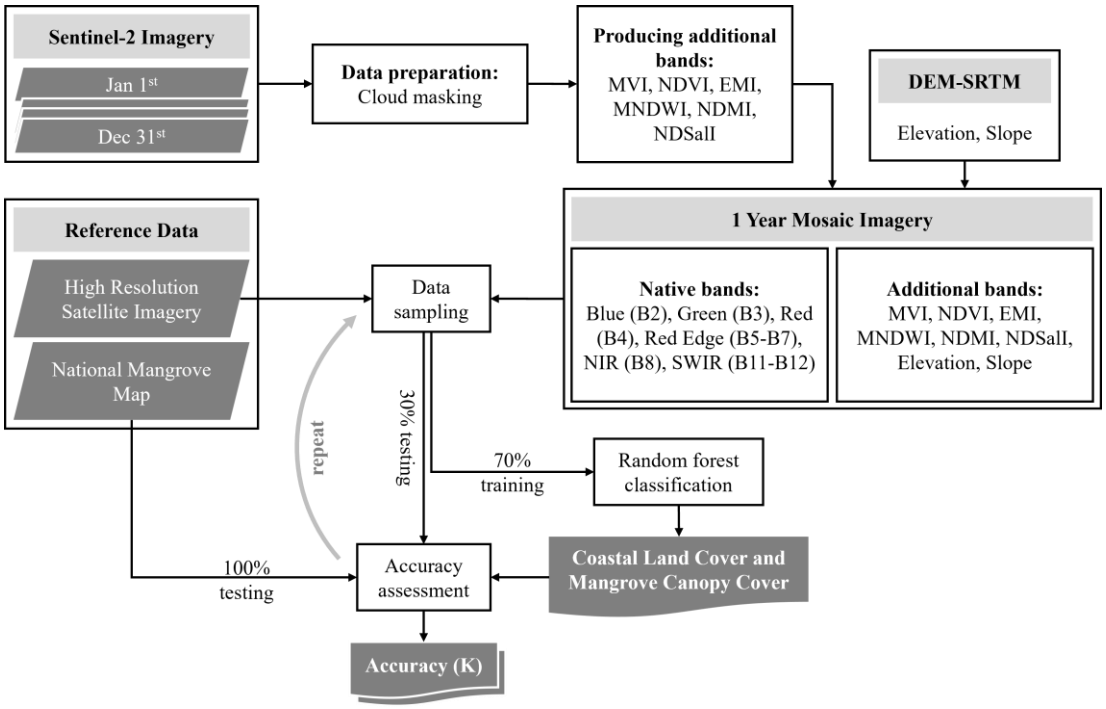

Figure 2-2: Research flow

3 RESULT AND DISCUSSION

3.1 Sentinel-2A RGB Visualization

Spectral analysis combining the Red (B4), NIR (B8), and SWIR (B11/B12) bands from Sentinel-2A imagery reveals distinct reflectance signatures across different coastal land cover types (Figure 3-1). Mangrove forests are characterized by low reflectance values in both the Red and SWIR bands, primarily due to their high leaf water content and tidal absorption effects. In contrast, the NIR band shows higher reflectance, reflecting a dense and healthy internal leaf structure (L. Wang et al., 2018; C. Zhang et al., 2012). Semi-natural terrestrial vegetation outside mangrove areas also shows high NIR reflectance, but generally higher SWIR values, which is caused by reduced leaf water content and drier soil conditions (Baloloy et al., 2020; L. Wang et al., 2018).

Open land areas, characterized by dry soils or sparse vegetation, typically show moderate reflectance in the Red band and redused values in the NIR, while the SWIR band exhibits intermediate reflectance levels indicating low moisture content (Tran et al., 2022; L. Wang et al., 2018). In contrast, built-up zones display high Red band reflectance due to the prevalence of artificial materials such as concrete and roofing, with relatively lower reflectance in the NIR and SWIR bands, and slightly higher reflectance in the Red and Green bands, especially in still water conditions, which facilitates their distinction from vegetated areas (Jia et al., 2019).

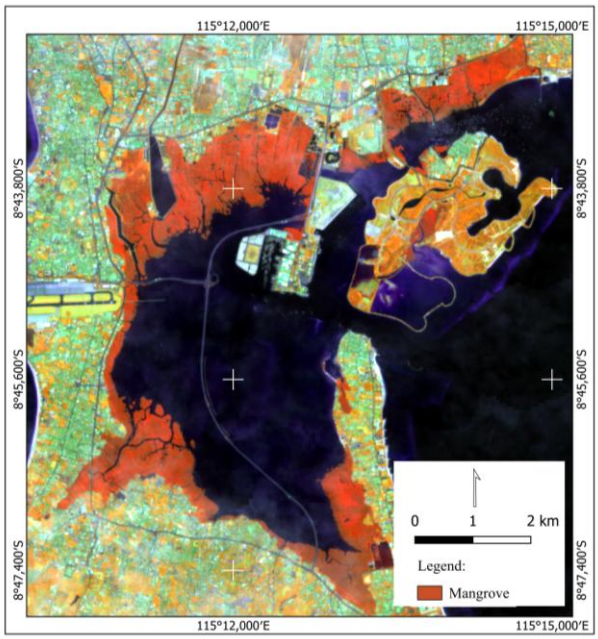

Figure 3-1: Mangrove view in RGB NIR SWIR Red from Sentinel-2A

By exploiting the spectral differences captured by these three bands, the RF algorithm effectively discriminates among coastal land cover types. The contrasting spectral differences between mangrove forests—characterized by low Red, high NIR, and low SWIR reflectance—and

terrestrial vegetation with high NIR and SWIR values, support better classification accuracy compared to relying solely on indices such as NDVI (Tran et al., 2022). This methodology has proven invaluable for accurately mapping coastal land cover in complex and dynamic tropical environments.

3.2 Coastal Land Cover Classification

The classification of coastal land cover in the Benoa Bay area using Sentinel-2A data combined with a RF algorithm demonstrated strong capability in distinguishing between complex land cover types such as mangroves, built-up land, water, and open lands (Figure 3-2). The RF model utilizes spectral information across the visible, near-infrared, and red-edge bands, enabling it to effectively separate classes with similar spectral signatures. Its non-parametric nature and robustness to multicollinearity among predictor variables make it well-suited to handling high-dimensional data commonly found in dynamic coastal zones. The overall classification accuracy exceeded 90%, with a Kappa statistic above 90%, highlighting the model's robustness in capturing spatial heterogeneity. These results corroborate previous research supporting RF as a reliable tool for coastal land cover mapping, particularly in tropical regions with diverse land use patterns (Belgiu & Drăguț, 2016; Panggabean et al., 2023; Rodriguez-Galiano et al., 2012).

In general, based on the results of land cover classification in the coastal area of Benoa Bay with different treatments (DS, wDS), there is a diverse spatial distribution between water classes, mangroves, non-mangrove vegetation, open land, and built-up land in locations that are not much different. Spatially, the classification map reveals distinct patterns: water (light blue) dominate the bay's central and canal areas, while mangroves (dark green) are predominantly found along shorelines and river deltas, particularly in the western and southeastern sectors, indicating dense forest cover. Non-mangrove vegetation (light green) tends to occupy upland zones adjacent to mangroves, extending beyond tidal limits. Open land (white) often appears near transitional areas between vegetation and urban development, possibly reflecting reclamation sites or vacant lands. Built-up areas (red) are concentrated primarily in the northern and northwestern parts, pointing to significant anthropogenic pressures on the coastal ecosystem.

Although the distribution of land cover class locations is in the exact location, there are differences in the area of land cover (Figure 3-2). The RF DS classification results show a wider range of mangrove and open land classes than the RF wDS results. The mangrove results of the RF DS cover 1,290 ha, while the RF wDS covers 1,270 ha. The open land of the RF DW is 2,022 ha, while the RF wDS covers 741 ha. In contrast to the land cover area for the water class, built-up land, and non-mangrove vegetation, the results of the RF DS classification are less than those of the RF wDS. The land cover of the water class from the RF DS covers an area of 6,158 ha, while the results of the RF wDS are 6,167 ha; the land cover of the built-up land class from the RF DS covers an area of 2,721 ha, while the results of the RF wDS are 2,889 ha. The land cover of the non-mangrove vegetation class from the RF DS covers an area of 2,243 ha, while the results of the RF wDS are 2,391 ha (Figure 3-3).

Based on the coastal land cover classification results in the Benoa Bay area, as presented in the confusion matrix, the accuracy metrics indicate that the classification model performs with high and consistent accuracy across different classes (Table 3-1 and Table 3-2).

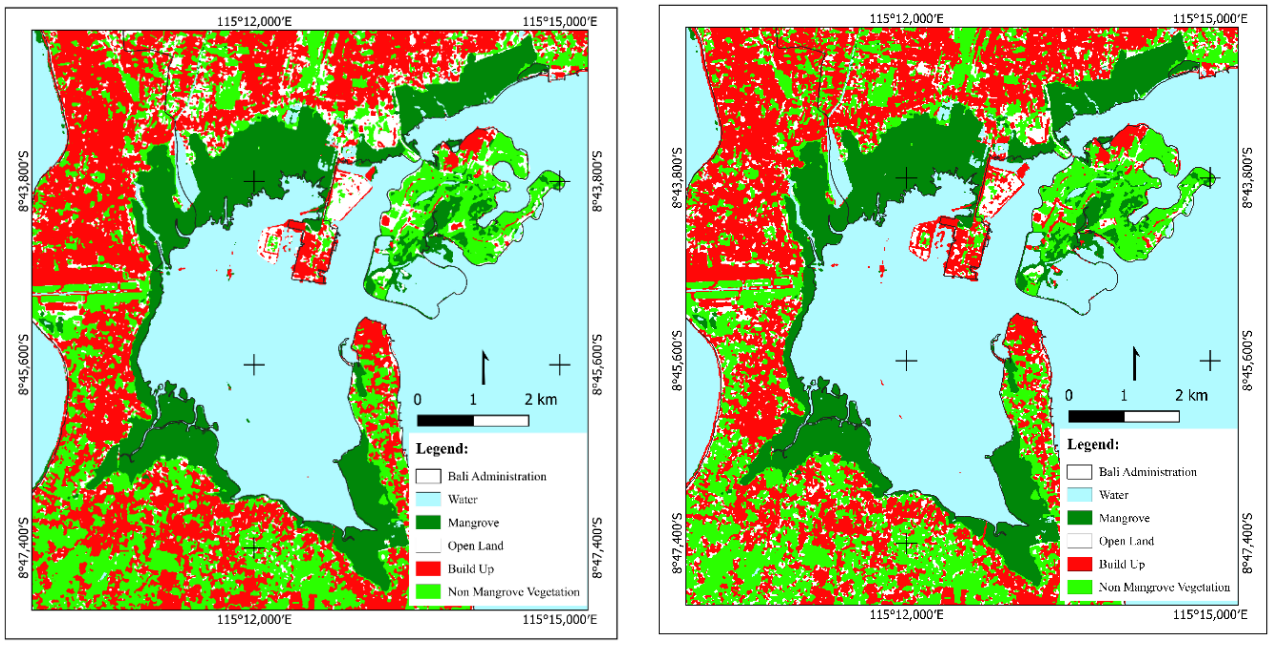

(a) (b)

Figure 3-2: Coastal land cover from the RF classification with DS (a) and wDS (b) treatment

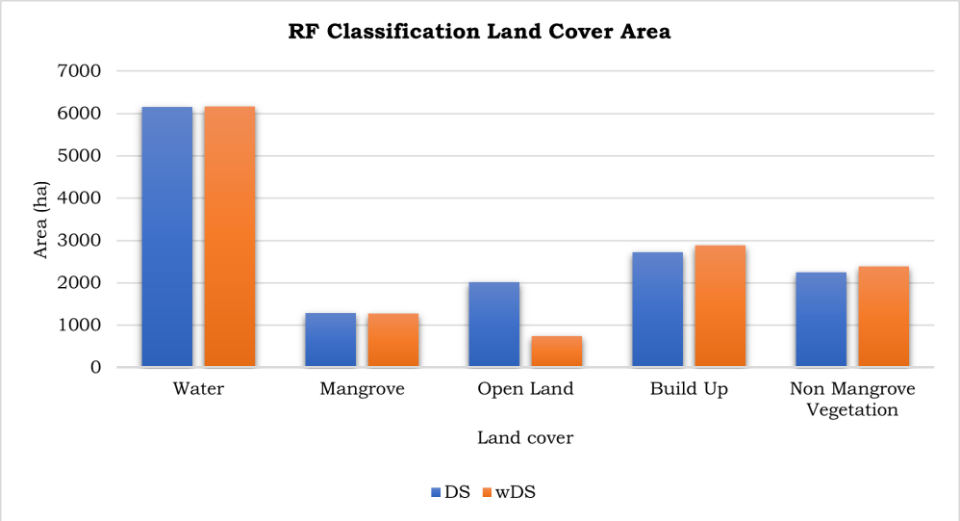

Figure 3-3: Land Cover Area with DS (a) and wDS (b) Treatment

Table 3-1: Confusion Matrix Accuracy Test of RF DS Classification

	Land Cover	Reference Data: Water	Mangrove	Open Land	Build Up	Non Mangrove Vegetation	Total	User Accuracy (%)
Class	Water	2,045	0	0	0	0	2,045	100
	Mangrove	0	912	0	0	0	912	100
	Open Land	1	0	174	1	1	177	98
	Build Up	0	0	6	898	0	904	99
	Non Mangrove Vegetation	0	0	5	1	310	316	98
Total		2,046	912	185	900	311	4,354	
Producer Accuracy (%)		100	100	94	100	100		
Overall Accuracy (OA) (%)								100
Kappa (K) (%)								99

Table 3-2: Confusion Matrix Accuracy Test of RF wDS Classification

		Reference Data						
	Land Cover	**Water**	**Mangrove**	**Open Land**	**Build Up**	**Non Mangrove Vegetation**	**Total**	**User Accuracy (%)**
Class	Water	2,088	0	0	0	0	2,088	100
	Mangrove	0	842	0	0	0	842	100
	Open Land	0	0	173	1	2	176	98
	Build Up	0	0	6	924	0	930	99
	Non Mangrove Vegetation	0	0	11	0	311	322	97
Total		2,088	842	190	925	313	4,358	
Producer Accuracy (%)		100	100	91	100	99		
Overall Accuracy (OA) (%)								100
Kappa (K) (%)								99

The water class shows user accuracies of 100% (2045/2045) and 100% (2088/2088) in DS and wDS classification, respectively, indicating that almost all pixels classified as water bodies are indeed water bodies according to the reference data. This high accuracy reflects the distinct spectral signature of water, particularly in the blue NIR bands, which are commonly used in remote sensing for water detection.

The mangrove class shows user accuracies of 100% (912/912) and 100% (842/842) in the DS and wDS classifications, respectively, indicating that the model is very effective at distinguishing mangroves from non-mangrove vegetation, even though ecologically both have overlapping reflectance spectral. This high performance suggests that the integration of vegetation indices and spectral features, such as NDVI, MVI, and SWIR bands, within the RF algorithm significantly enhances the precision in identifying coastal vegetation types.

The open land class had user accuracies of 98% (174/177) and 98% (173/176) in DS and wDS classification, respectively. Although slightly lower than the water and mangrove classes, this result remains high and indicates that areas with minimal or no vegetation cover are relatively easy for the model to identify. The strong reflectance differences in the SWIR and Red bands contribute to the model's ability to distinguish this class from vegetated areas.

In the build-up class, user accuracy in the DS and wDS classifications was 99% (898/904) and 99% (924/930), respectively, indicating high accuracy in classifying built-up areas. High reflectance in the SWIR band and distinct textural roughness serve as key indicators that allow the RF algorithm to effectively classify this land cover type.

The non-mangrove vegetation class showed user accuracy in the DS and wDS classification of 98% (310/316) and 97% (311/322), slightly lower than mangrove, but still relatively accurate. This suggests that despite spectral similarities with mangrove, the inclusion of additional spectral and textural features successfully minimized classification errors and improved overall model performance.

Overall, the accuracy is 100%, with 4339 out of 4354 pixels correctly classified in RF DS and 4338 out of 4358 in RF wDS. The high overall and per-class accuracy confirms that the RF algorithm, which uses a combination of multiband Sentinel 2A data and relevant spectral indices, effectively identified land cover variations in ecologically complex coastal areas such as Benoa Bay.

This spatial distribution pattern highlights the need for further analysis on habitat fragmentation and ecological connectivity of mangrove ecosystems, particularly in response to the ongoing expansion of built-up areas. The satellite

image-based classification approach provides accurate and up-to-date information, which is essential for supporting data-driven coastal conservation planning and sustainable management efforts.

3.3 Mangrove Canopy Cover

Different spectral reflectance patterns enable effective differentiation among vegetation, soil, and water in satellite-based land cover classification. The red spectral region (600–700 nm) is highly responsive to chlorophyll absorption, resulting in low reflectance values for healthy vegetation. Conversely, vegetation tends to reflect strongly in the NIR spectrum (700–1100 nm) due to its internal leaf structure, which scatters NIR wavelengths efficiently (H. Zhang et al., 2023). In the SWIR region (beyond 1100 nm), reflectance is primarily influenced by water content and the structural composition of plant material, such as cellulose. Vegetation with high moisture levels, including mangroves, typically exhibits strong SWIR absorption. As such, the spectral signature characterized by high NIR reflectance and reduced SWIR reflectance serves as a key indicator of healthy, water-rich foliage commonly associated with mangrove ecosystems (C. Zhang et al., 2012).

In mangrove vegetation located in the intertidal zones, NIR reflectance is very high, while SWIR and Red reflectance are quite low, resulting in a distinctive spectral profile—usually appearing dark brown or dark green in the image. This pattern results from tidal inundation, which increases moisture in both leaf tissues and substrate, enhancing SWIR absorption and generating strong contrast with high NIR reflectance (Prayudha et al., 2024; H. Zhang et al., 2023). The simultaneous use of these bands in spectral index-based classifications, such as NDVI or MVI, is highly effective in distinguishing mangrove cover from other coastal vegetation, especially in complex ecotonal environments.

Overlay results between mangrove canopy cover from the RF DS and WDS classifications and the national mangrove map show a high degree of spatial agreement. The mangrove canopy cover shown in dark green is mainly within the boundaries of the national mangrove map, marked by the yellow line. However, several areas of mangrove canopy are identified as being outside the official boundaries of the national map, indicating possible spatial changes or previously unmapped natural expansion of mangroves (Figure 3-4). In addition, errors occur in water pools or puddles that are detected as mangroves, possibly because these objects resemble the reflections of mangroves that grow in flooded areas.

Based on the resulting confusion matrix, the RF DS classification showed high accuracy with a user accuracy of 82% for the mangrove class (105,264 of 128,659 pixels), and RF wDS of 83% (105,197 of 126,601 pixels), indicating that most of the pixels classified as mangroves were indeed in accordance with the national reference map. The non-mangrove class also showed high accuracy of 100% (1,243,938 of 1,249,754 pixels) in the RF DS classification and 100% (1,245,929 of 1,252,812 pixels) in the RF wDS classification, reflecting the model's ability to distinguish areas not covered by mangroves.

Overall, the total number of correctly classified pixels in RF DS was 1,349,202 out of 1,378, 413, resulting in an overall accuracy of 98%; in RF wDS, 1,351,126 out of 1,378,413 pixels, with an overall accuracy of 98%. This level of accuracy indicates that the Sentinel-2 data-based classification approach with the RF algorithm can accurately identify mangrove canopies, even at a higher level of detail than the national reference. The emerging spatial differences may indicate the actual dynamics of mangrove cover, requiring regular updates to the reference map based on the latest observational data.

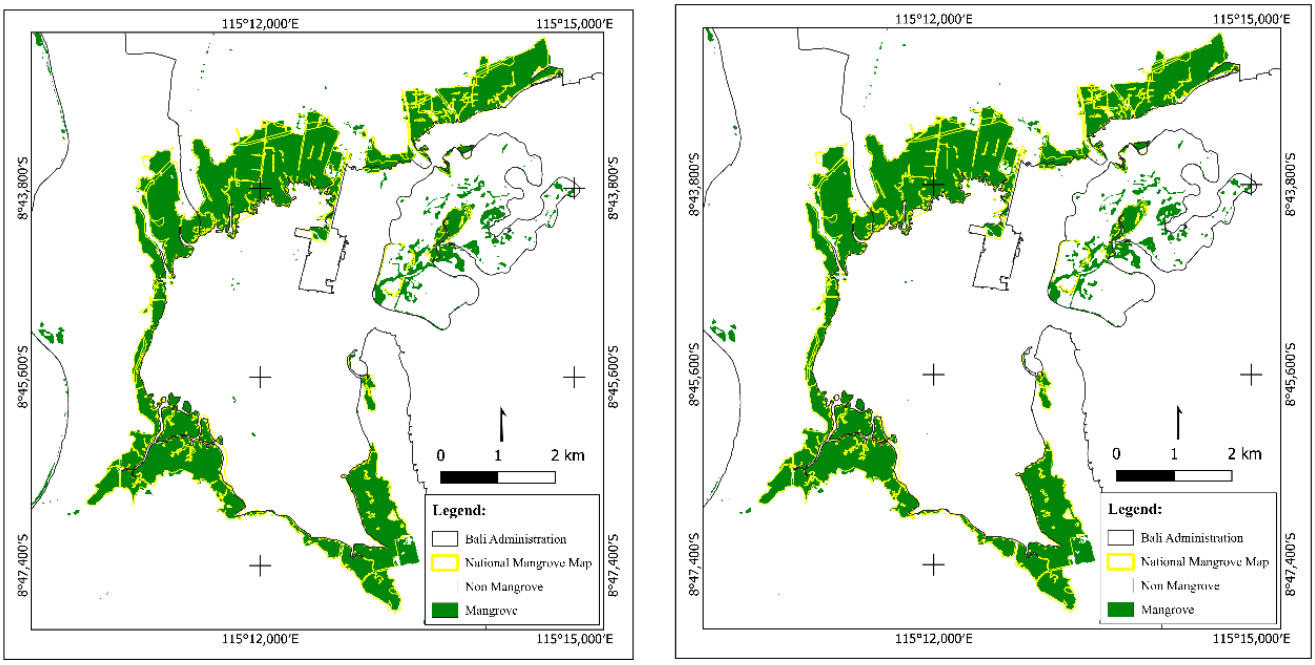

(a) (b)

Figure 3-4 : Overlay results of the 2024 National Mangrove Map with mangrove canopy cover results from RF DS (a) and RF wDS (b)

Table 3-3: Accuracy Test of RF DS Classification Confusion Matrix with National Mangrove Map

Land Cover		Reference Data		Total	User Accuracy (%)
		Non-mangrove	Mangrove		
Class	Non-mangrove	1,243,938	5,816	1,249,754	100
	Mangrove	23,395	105,264	128,659	82
Total		1,267,333	111,080	1,378,413	
Producer Accuracy (%)		98	95		
Overall Accuracy (OA) (%)				98	
Kappa (K) (%)				87	

Table 3-3: Accuracy Test of RF wDS Classification Confusion Matrix with National Mangrove Map

Land Cover		Reference Data		Total	User Accuracy (%)
		Non-mangrove	Mangrove		
Class	Non-mangrove	1,245,929	5,883	1,251,812	100
	Mangrove	21,404	10,5197	126,601	83
Total		1,267,333	111,080	1,378,413	
Producer Accuracy (%)		98	95		
Overall Accuracy (OA) (%)				98	
Kappa (K) (%)				87	

3.4 Discussion

In this study, mangrove canopy cover classification was performed using the RF algorithm, combined with several spectral indices (NDVI, MVI, MNDWI, EMI, and NDSaII) in Sentinel-2A data, demonstrating strong capability in minimizing spectral confusion between mangroves and other coastal vegetation types. NDVI is widely recognized for its responsiveness to vegetation greenness and exhibits a high correlation with mangrove canopy area ($r \approx 0.91$), as noted by (Xue & Qian, 2022). However, it remains insufficient to distinguish mangroves from other dense green cover reliably. More targeted indices, such as MVI and EMI, have demonstrated superior performance in capturing distinct spectral and structural features of various mangrove communities (Baloloy et al., 2020; Prayudha et al., 2024). In particular, EMI can accurately separate mangrove species, including nipa palms and forest floor components, achieving an overall classification accuracy of 87% and a Kappa value of 0.84. These results surpass those obtained using the standard RF classification method (OA = 0.73, Kappa = 0.66) and also outperform other indices such as AMMI, according to (Prayudha et al., 2024).

The MVI was specifically designed to enhance mapping accuracy in mangrove ecosystems by contrasting NIR–Green and SWIR–Green reflectance values, which improves the separation of mangroves from both coastal vegetation and bare surfaces (Baloloy et al., 2020). Furthermore, a suite of moisture-sensitive indices—namely MNDWI, EMI, and NDSaII—adds depth to the analysis by detecting wetness and salinity gradients that are not captured by NDVI alone. For example, MNDWI and NDMI reveal surface water presence and soil moisture content, crucial for distinguishing mangrove zones (Simarmata et al., 2024). Meanwhile, NDSaII plays an important role in determining saline microhabitats, thus supporting accurate mapping of mangrove stands in coastal areas (Parenti, 2014).

Recent research highlights that integrating time-series features from vegetation and water-related indices, particularly NDVI and MNDWI, can significantly enhance the performance of land cover classification using the RF algorithm. Reported gains in accuracy reach up to 94%, representing a notable improvement from baseline levels of around 82% (Arfa & Minaei, 2024). One of RF's key strengths lies in its ability to manage multicollinearity and handle high-dimensional datasets comprising diverse spectral and structural features, all while maintaining consistent classification quality (Raza et al., 2024; Waśniewski et al., 2020).

Coastal vegetation has similar spectral signatures—especially in NDVI values or texture characteristics—making misclassification a common problem; however, RF's ability to integrate multi-source inputs helps mitigate these errors by leveraging complementary data dimensions. This advantage is particularly evident in complex ecosystems such as mangroves, where spectral overlap is common. Furthermore, RF algorithms have demonstrated robustness across multiple image segmentation scales and in noisy or imbalanced training datasets, provided the training samples are of sufficient size and diversity (Cherian & K, 2024; Maurya et al., 2021).

The addition of texture-based features, particularly those derived from the Grey-Level Co-Occurrence Matrix (GLCM), further enhanced classification accuracy. High-resolution imagery, such as that from WorldView-3, has proven effective in differentiating among mangrove species when combined with spectral and textural inputs (T. Wang et al., 2015).

In mangrove ecosystems, microtopography—especially surface elevation and slope—plays a critical role in determining tidal inundation regimes that shape spatial patterns of vegetation zonation. Elevation functions as a reliable proxy for flood frequency and duration, thereby indirectly influencing soil salinity, texture, and redox conditions that govern mangrove community distributions (Baloloy et al., 2020; Leong et al., 2018). Moreover, slope geometry—whether concave or convex—affects tidal flow and sediment deposition dynamics, ultimately modulating habitat resilience to sea-level rise and the formation of distinct intertidal zones (Xie et al., 2022). Although elevation and slope play an essential role in mangrove growth, this study did not find a significant effect due to differences in the spatial resolution of the image data used.

Elevation and slope data from the 30 m resolution SRTM DEM did not significantly influence the results compared to higher-resolution image data because, in reality, there are various topographic height variations within 30 m pixels. Therefore, for accurate results, elevation and topographic data with more detailed spatial resolution are required.

Recent evidence indicates that integrating vegetation, moisture/salinity indices, and terrain variables (elevation and slope) within RF models markedly improves mangrove mapping accuracy, particularly for canopy extent and coastal land cover delineation. For instance, studies by (Ligono & Okolie, 2022) demonstrated enhanced detection of mangrove changes in Gambia when MVI and RF were combined. Similarly, (Simarmata et al., 2024) observed that incorporating indices such as EMI and NDSaII allowed RF to capture moisture content and salinity gradients unique to mangrove environments more effectively.

Furthermore, integrating structural features (e.g. GLCM-derived texture) and SAR data—such as Sentinel-1 backscatter—can significantly boost classification precision by providing information on canopy structure and subsurface moisture not fully represented in optical imagery alone (Cherian & K, 2024; Simarmata et al., 2024). This research addresses the gap in understanding RF's robustness to spectral overlap by proposing a comprehensive approach combining spectral, textural, and moisture-related inputs—offering an adaptive framework for reliable mangrove canopy detection.

Despite its advantages, RF classification still classifies some water bodies, ponds, or puddles as mangroves. This error is caused by the complex interactions among the training data structure, limited image resolution, spectral characteristics of coastal areas, tidal conditions, and the lack of ecological information during modeling, as RF performs separation based on spectral features or indices (Xia et al., 2018). Classification of coastal objects using RF requires selecting appropriate inputs, as the coastal environment is influenced by dynamic tides that affect water spectral values. Water bodies, ponds, and puddles in coastal areas contain a mixture of water, sediment, and algae or similar organisms, thus having reflectance values identical to those of mangroves. Therefore, RF misidentifies these objects due to the lack of clear boundaries between these features (A. Zhang et al., 2019). Differences in tidal phases affect spectral values, so classification on a single recording date can provide less or more information; therefore, it is recommended to use multitemporal data (Xia et al., 2018).

4 CONCLUSSIONS

This research concludes that the RF algorithm demonstrates strong capability in classifying coastal land cover, particularly in accurately identifying mangrove canopy cover at a spatial scale. The developed model, which integrates Sentinel-2A data along with a combination of spectral bands and vegetation indices, yielded high classification performance. Accuracy assessment indicated high values of overall accuracy and Kappa coefficient for coastal land cover classification, as well as for mangrove canopy mapping when validated against the 2024 national mangrove map. These results confirm that the proposed approach is reliable and suitable for supporting sustainable monitoring and management of coastal areas.

ACKNOWLEDGMENT

This research was conducted by the grant from National Research and Innovation Agency (BRIN) through Degree by Research program.

REFERENCES

Anggraeni, I. D. (2024). The Role Of Regulations In Supporting The Restoration Of Mangrove Ecosystems For The Achievement Of Sustainable Development Goals: A Literature Review. *Eduvest - Journal of Universal Studies*, *4*(11), 10361–10378. https://doi.org/10.59188/eduvest.v4i11.43690

Arfa, A., & Minaei, M. (2024). Utilizing multitemporal indices and spectral bands of Sentinel-2 to enhance land use and land cover classification with random forest and support vector machine. *Advances in Space Research*, *74*(11), 5580–5590.

https://doi.org/10.1016/j.asr.2024.08.062

As-syakur, Abd. R., Setiawati, M. D., Novanda, I. G. A., Rachman, H. A., Wirayuda, I. K. A. K., Aryunisha, P. E. P., Saifulloh, Moh., & Pratama, R. T. (2025). Spatio-Temporal Variation Trends of Mangrove Canopy Cover in Urban Areas Using Landsat 8 Imagery and Implications of Management Policies: A Case Study of the Benoa Bay Mangrove Area, Bali, Indonesia. *Wild*, *2*(1), 8. https://doi.org/10.3390/wild2010008

Bachmid, F., Sondak, C., & Kusen, J. (2018). Estimasi penyerapan karbon hutan mangrove Bahowo Kelurahan Tongkaina Kecamatan Bunaken. *JURNAL PESISIR DAN LAUT TROPIS*, *6*(1), 8. https://doi.org/10.35800/jplt.6.1.2018.19463

Bali (Denpasar) Climate (Indonesia): Data and Graphs for Weather & Climate In Bali (Denpasar). (2025). [Dataset]. https://en.climate-data.org/asia/indonesia/bali/bali-denpasar-3427/

Baloloy, A. B., Blanco, A. C., Sta. Ana, R. R. C., & Nadaoka, K. (2020). Development and application of a new mangrove vegetation index (MVI) for rapid and accurate mangrove mapping. *ISPRS Journal of Photogrammetry and Remote Sensing*, *166*, 95–117. https://doi.org/10.1016/j.isprsjprs.2020.06.001

Belgiu, M., & Drăguț, L. (2016). Random forest in remote sensing: A review of applications and future directions. *ISPRS Journal of Photogrammetry and Remote Sensing*, *114*, 24–31. https://doi.org/10.1016/j.isprsjprs.2016.01.011

Biau, G., & Scornet, E. (2016). A random forest guided tour. *TEST*, *25*(2), 197–227. https://doi.org/10.1007/s11749-016-0481-7

Breiman, L. (2001). Random Forests. *Machine Learning*, *45*(1), 5–32. https://doi.org/10.1023/A:1010933404324

Castillo, Y. B., Kim, K., & Kim, H. S. (2021). Thirty-two years of mangrove forest land cover change in Parita Bay, Panama. *Forest Science and Technology*, *17*(2), 67–79. https://doi.org/10.1080/21580103.2021.1922512

Cherian, S. M., & K, R. (2024). Random forest and support vector machine classifiers for coastal wetland characterization using the combination of features derived from optical data and synthetic aperture radar dataset. *Journal of Water and Climate Change*, *15*(1), 29–49. https://doi.org/10.2166/wcc.2023.238

Congalton, R. G. (1991). A review of assessing the accuracy of classifications of remotely sensed data. *Remote Sensing of Environment*, *37*(1), 35–46. https://doi.org/10.1016/0034-4257(91)90048-B

Danaparamita, E. D. (2020). Dukungan Sosial Terhadap Manajemen Pelestarian Lingkungan Kawasan Ekowisata Mangrove Taman Hutan Raya Ngurah Rai, Bali. *Jurnal Green Growth Dan Manajemen Lingkungan*, *8*(1), 38–43. https://doi.org/10.21009/jgg.081.04

Donato, D. C., Kauffman, J. B., Murdiyarso, D., Kurnianto, S., Stidham, M., & Kanninen, M. (2011). Mangroves among the most carbon-rich forests in the tropics. *Nature Geoscience*, *4*(5), 293–297. https://doi.org/10.1038/ngeo1123

Elmahdy, S. I., Ali, T. A., Mohamed, M. M., Howari, F. M., Abouleish, M., & Simonet, D. (2020). Spatiotemporal Mapping and Monitoring of Mangrove Forests Changes From 1990 to 2019 in the Northern Emirates, UAE Using Random Forest, Kernel Logistic Regression and Naive Bayes Tree Models. *Frontiers in Environmental Science*, *8*, 102. https://doi.org/10.3389/fenvs.2020.00102

ESA. (2025). *ESA - Sentinel-2*. European Space Agency. https://www.esa.int/Applications/Observing_the_Earth/Copernicus/Sentinel-2

Friess, D. A., Rogers, K., Lovelock, C. E., Krauss, K. W., Hamilton, S. E., Lee, S. Y., Lucas, R., Primavera, J., Rajkaran, A., & Shi, S. (2019). The State of the World's Mangrove Forests: Past, Present, and Future. *Annual Review of Environment and Resources*, *44*(1), 89–115. https://doi.org/10.1146/annurev-environ-101718-033302

Gilani, H., Naz, H. I., Arshad, M., Nazim, K., Akram, U., Abrar, A., & Asif, M. (2021). Evaluating mangrove conservation and sustainability through spatiotemporal (1990–2020) mangrove cover change analysis in Pakistan. *Estuarine, Coastal and Shelf Science*, *249*, 107128. https://doi.org/10.1016/j.ecss.2020.107128

Giri, C. (2023). Frontiers in Global Mangrove Forest Monitoring. *Remote Sensing*,

15(15), 3852. https://doi.org/10.3390/rs15153852

Gong, M., Teller, N., Golebie, E. J., Aczel, M., Jiang, Z., Van Zeghbroeck, J., & Liu, J. (2024). Unveiling complementarities between mangrove restoration and global sustainable development goals. *Journal of Cleaner Production*, *474*, 143524. https://doi.org/10.1016/j.jclepro.2024.143524

Immitzer, M., Atzberger, C., & Koukal, T. (2012). Tree Species Classification with Random Forest Using Very High Spatial Resolution 8-Band WorldView-2 Satellite Data. *Remote Sensing*, *4*(9), 2661–2693. https://doi.org/10.3390/rs4092661

Jia, M., Wang, Z., Wang, C., Mao, D., & Zhang, Y. (2019). A New Vegetation Index to Detect Periodically Submerged Mangrove Forest Using Single-Tide Sentinel-2 Imagery. *Remote Sensing*, *11*(17), 2043. https://doi.org/10.3390/rs11172043

Kauffman, J. B., Adame, M. F., Arifanti, V. B., Schile-Beers, L. M., Bernardino, A. F., Bhomia, R. K., Donato, D. C., Feller, I. C., Ferreira, T. O., Jesus Garcia, M. D. C., MacKenzie, R. A., Megonigal, J. P., Murdiyarso, D., Simpson, L., & Hernández Trejo, H. (2020). Total ecosystem carbon stocks of mangroves across broad global environmental and physical gradients. *Ecological Monographs*, *90*(2). https://doi.org/10.1002/ecm.1405

Kuenzer, C., Bluemel, A., Gebhardt, S., Quoc, T. V., & Dech, S. (2011). Remote Sensing of Mangrove Ecosystems: A Review. *Remote Sensing*, *3*(5), 878–928. https://doi.org/10.3390/rs3050878

Leong, R. C., Friess, D. A., Crase, B., Lee, W. K., & Webb, E. L. (2018). High-resolution pattern of mangrove species distribution is controlled by surface elevation. *Estuarine, Coastal and Shelf Science*, *202*, 185–192. https://doi.org/10.1016/j.ecss.2017.12.015

Ligono, L. K., & Okolie, C. J. (2022). Integrated Analysis of Mangrove Changes Using The Mangrove Vegetation Index and Random Forest Classification in The Gambia. *The International Archives of the Photogrammetry, Remote Sensing and Spatial Information Sciences*, *XLVI-M-2–2022*, 153–157. https://doi.org/10.5194/isprs-archives-xlvi-m-2-2022-153-2022

Loviasari, N. W., As-syakur, Abd. R., Faiqoh, E., Dirgayusa, I. G. N. P., & Wiyanto, D. B. (2017). Struktur Komunitas Uca Sp Di Kawasan Teluk Benoa Pada Karakteristik Substrat Yang Berbeda. *Journal of Marine and Aquatic Sciences*, *4*(1), 141. https://doi.org/10.24843/jmas.2018.v4.i01.141-150

Maurya, K., Mahajan, S., & Chaube, N. (2021). Remote sensing techniques: Mapping and monitoring of mangrove ecosystem—a review. *Complex & Intelligent Systems*, *7*(6), 2797–2818. https://doi.org/10.1007/s40747-021-00457-z

Ministry of Forestry. (2025). *National Mangrove Map 2024* [Map].

Mukherjee, N., Sutherland, W. J., Dicks, L., Hugé, J., Koedam, N., & Dahdouh-Guebas, F. (2014). Ecosystem Service Valuations of Mangrove Ecosystems to Inform Decision Making and Future Valuation Exercises. *PLoS ONE*, *9*(9), e107706. https://doi.org/10.1371/journal.pone.0107706

Murdiyarso, D., Purbopuspito, J., Kauffman, J. B., Warren, M. W., Sasmito, S. D., Donato, D. C., Manuri, S., Krisnawati, H., Taberima, S., & Kurnianto, S. (2015). The potential of Indonesian mangrove forests for global climate change mitigation. *Nature Climate Change*, *5*(12), 1089–1092. https://doi.org/10.1038/nclimate2734

Nandika, M. R., Suardana, A. A. Md. A. P., & Anggraini, N. (2023). Mapping of Mangrove using Multivariate Random Forest Algorithm, Case Study in Segara Anakan, Cilacap. *Majalah Ilmiah Globe*, *25(1)*, 21–30.

Panggabean, H. L. R., Susilo, H., Nanda Pratama, R., Irawan, B., Masfiroh, S., Nofrianda Ilyas, G., Oktorini, Y., & Jhonnerie, R. (2023). Spatial mapping and temporal dynamics of mangrove: A case study in 'pro-mangrove' villages, Indragiri Hilir District, Indonesia. *BIO Web of Conferences*, *74*, 03002. https://doi.org/10.1051/bioconf/20237403002

Parenti, M. S. (2014). *Hurricane Effects on Mangrove Canopies Observed from MODIS and SPOT Imagery* (Version 3). arXiv. https://doi.org/10.48550/ARXIV.1412.2201

Prayudha, B., Ulumuddin, Y. I., Siregar, V., Suyarso, Agus, S. B., Prasetyo, L. B., Suyadi, Avianto, P., & Ramadhani, M. R. (2024). Enhanced mangrove index: A spectral index for discrimination understorey, nypa, and mangrove trees. *MethodsX*, *12*, 102778.

https://doi.org/10.1016/j.mex.2024.102778

Purwanto, A. D., Wikantika, K., Deliar, A., & Darmawan, S. (2022). Decision Tree and Random Forest Classification Algorithms for Mangrove Forest Mapping in Sembilang National Park, Indonesia. *Remote Sensing*, *15*(1), 16. https://doi.org/10.3390/rs15010016

Raza, S. A., Zhang, L., Zuo, J., & Chen, B. (2024). Time series monitoring and analysis of Pakistan's mangrove using Sentinel-2 data. *Frontiers in Environmental Science*, *12*. https://doi.org/10.3389/fenvs.2024.1416450

Rodriguez-Galiano, V. F., Chica-Olmo, M., Abarca-Hernandez, F., Atkinson, P. M., & Jeganathan, C. (2012). Random Forest classification of Mediterranean land cover using multi-seasonal imagery and multi-seasonal texture. *Remote Sensing of Environment*, *121*, 93–107. https://doi.org/10.1016/j.rse.2011.12.003

Sasmito, S. D., Basyuni, M., Kridalaksana, A., Saragi-Sasmito, M. F., Lovelock, C. E., & Murdiyarso, D. (2023). Challenges and opportunities for achieving Sustainable Development Goals through restoration of Indonesia's mangroves. *Nature Ecology & Evolution*, *7*(1), 62–70. https://doi.org/10.1038/s41559-022-01926-5

Simarmata, N., Wikantika, K., Darmawan, S., Harto, A. B., Sakti, A. D., & Santo, A. A. (2024). Mangrove ecosystem species mapping from integrated Sentinel-2 imagery and field spectral data using random forest algorithm. *Journal of Applied Remote Sensing*, *18*(01). https://doi.org/10.1117/1.jrs.18.014509

Sugianthi, N. L. M. A., Arthana, I. W., & Adnyana, I. W. S. (2007). Monitoring Mangrove Area in Benoa Bay Using Landsat TM AND ETM + Data. *ECOTROPHIC*, *2(1)*, 1–10.

Tomlinson, P. B. (2016). *The Botany of Mangroves*. Cambridge University Press.

Tran, T. V., Reef, R., & Zhu, X. (2022). A Review of Spectral Indices for Mangrove Remote Sensing. *Remote Sensing*, *14*(19), 4868. https://doi.org/10.3390/rs14194868

Wahyudi, A. J., Afdal, Adi, N. S., Rustam, A., Hadiyanto, Rahmawati, S., Irawan, A., Dharmawan, I. W. E., Prayudha, B., Hafizt, M., Prayitno, H. B., Rahayu, Y. P., Solihudin, T., Ati, R. N. A. A., Kepel, T. L., K, M. A., Daulat, A., Salim, H. L., Sudirman, N., … Supriyadi, I. H. (2018). *Potensi Cadangan dan Serapan Karbon Ekosistem Mangrove dan Padang Lamun Indonesia*.

Wang, L., Fan, H., & Wang, Y. (2018). Estimation of consumption potentiality using VIIRS night-time light data. *PLOS ONE*, *13*(10), e0206230. https://doi.org/10.1371/journal.pone.0206230

Wang, T., Zhang, H., Lin, H., & Fang, C. (2015). Textural–Spectral Feature-Based Species Classification of Mangroves in Mai Po Nature Reserve from Worldview-3 Imagery. *Remote Sensing*, *8*(1), 24. https://doi.org/10.3390/rs8010024

Waśniewski, A., Hościło, A., Zagajewski, B., & Moukétou-Tarazewicz, D. (2020). Assessment of Sentinel-2 Satellite Images and Random Forest Classifier for Rainforest Mapping in Gabon. *Forests*, *11*(9), 941. https://doi.org/10.3390/f11090941

Xia, Q., Qin, C.-Z., Li, H., Huang, C., & Su, F.-Z. (2018). Mapping Mangrove Forests Based on Multi-Tidal High-Resolution Satellite Imagery. *Remote Sensing*, *10*(9), 1343. https://doi.org/10.3390/rs10091343

Xie, D., Schwarz, C., Kleinhans, M. G., Zhou, Z., & Van Maanen, B. (2022). Implications of Coastal Conditions and Sea-Level Rise on Mangrove Vulnerability: A Bio-Morphodynamic Modeling Study. *Journal of Geophysical Research: Earth Surface*, *127*(3). https://doi.org/10.1029/2021jf006301

Xu, H. (2006). Modification of normalised difference water index (NDWI) to enhance open water features in remotely sensed imagery. *International Journal of Remote Sensing*, *27*(14), 3025–3033. https://doi.org/10.1080/01431160600589179

Xue, Z., & Qian, S. (2022). Generalized Composite Mangrove Index for Mapping Mangroves Using Sentinel-2 Time Series Data. *IEEE Journal of Selected Topics in Applied Earth Observations and Remote Sensing*, *15*, 5131–5146. https://doi.org/10.1109/jstars.2022.3185078

Yastika, P. E., Shimizu, N., & Abidin, H. Z. (2019). Monitoring of long-term land subsidence from 2003 to 2017 in coastal area of Semarang, Indonesia by SBAS DInSAR analyses using Envisat-ASAR, ALOS-PALSAR, and Sentinel-1A SAR data. *Advances in Space Research*, *63*(5), 1719–1736.

https://doi.org/10.1016/j.asr.2018.11.008

Zhang, A., Sun, G., Ma, P., Jia, X., Ren, J., Huang, H., & Zhang, X. (2019). Coastal Wetland Mapping with Sentinel-2 MSI Imagery Based on Gravitational Optimized Multilayer Perceptron and Morphological Attribute Profiles. *Remote Sensing*, *11*(8), 952. https://doi.org/10.3390/rs11080952

Zhang, C., Liu, Y., Kovacs, J. M., Flores-Verdugo, F., Flores de Santiago, F., & Chen, K. (2012). Spectral response to varying levels of leaf pigments collected from a degraded mangrove forest. *Journal of Applied Remote Sensing*, *6*(1), 063501. https://doi.org/10.1117/1.jrs.6.063501

Zhang, H., Xia, Q., Dai, S., Zheng, Q., Zhang, Y., & Deng, X. (2023). Mangrove forest mapping from object-oriented multi-feature ensemble classification using Sentinel-2 images. *Frontiers in Marine Science*, *10*. https://doi.org/10.3389/fmars.2023.1243116